

Angle-differential cross sections for Rayleigh scattering of highly linearly polarized hard x rays on Au atoms

Wilko Middents ^{1,2,*} Günter Weber ^{2,3} Alexandre Gumberidze ³ Christoph Hahn ^{2,3} Thomas Krings ⁴
 Nikolaus Kurz ³ Philip Pfäfflein ^{2,3} Norbert Schell ⁵ Uwe Spillmann ³ Sophia Strnat ^{6,7} Marco Vockert,^{1,2}
 Andrey Volotka ² Andrey Surzhykov ^{6,7} and Thomas Stöhlker ^{1,2,3}

¹*Institute of Optics and Quantum Electronics, Friedrich Schiller University Jena, Max-Wien-Platz 1, 07743 Jena, Germany*

²*Helmholtz Institute Jena, Fröbelstieg 3, 07743 Jena, Germany*

³*GSI Helmholtzzentrum für Schwerionenforschung GmbH, Planckstraße 1, 64291 Darmstadt, Germany*

⁴*Institut für Kernphysik, Forschungszentrum Jülich, 52425 Jülich, Germany*

⁵*Institute of Materials Physics, Helmholtz-Zentrum Hereon, Max-Planck-Straße 1, 21502 Geesthacht, Germany*

⁶*Physikalisch-Technische Bundesanstalt, 38116 Braunschweig, Germany*

⁷*Technische Universität Braunschweig, 38106 Braunschweig, Germany*



(Received 17 October 2022; accepted 23 November 2022; published 9 January 2023; corrected 25 May 2023)

We perform a study on Rayleigh scattering of highly linearly polarized hard x rays on a thin Au foil target. In the study the angular distribution of the scattered radiation is analyzed in a relativistic regime both within and out of the plane of polarization of the incident beam. Within this experiment we scatter a synchrotron beam with a photon energy of 175 keV on a high-Z target foil, namely, gold. Our findings correlate well with state-of-the-art calculations of the scattering process performed in the framework of quantum electrodynamics and may have considerable impact on future experiments regarding a polarization-resolved analysis of Delbrück scattering. Furthermore, we show that the angular distribution of Rayleigh scattering can be used for a highly sensitive determination of the degree and orientation of the linear polarization of the incident hard-x-ray beam, if we rely on the theoretical framework.

DOI: [10.1103/PhysRevA.107.012805](https://doi.org/10.1103/PhysRevA.107.012805)

I. INTRODUCTION

Elastic photon scattering refers to photon-matter interaction processes in which both the incident and scattered photons carry the same energy $\hbar\omega$. It comprises a number of distinct interaction mechanisms: Scattering from bound electrons is referred to as Rayleigh scattering [1] and dominates the total elastic scattering cross section in a broad energy range from a few keV up to the MeV range. At higher photon energies, scattering from vacuum fluctuations in the nuclear field (Delbrück scattering [2]) and nuclear scattering processes, namely, nuclear Thomson scattering [3] and nuclear resonance scattering [4], become important. Comprehensive reviews on the topic of elastic x-ray scattering by atoms have been given by, e.g., Kane *et al.* [5] and Bradley *et al.* [6].

Early experimental studies of elastic photon scattering in the high-energy domain usually used intense unpolarized γ sources to provide the incident radiation and were mainly focusing on total and angle-differential cross-section measurements [5,7–9]. However, a complete characterization of

the scattering process has to account not only for the scattering cross section, but also for the photon polarization characteristics. In polarization-resolved experimental studies a much more detailed test of the theoretical approaches can be achieved.

A drawback of using the aforementioned γ sources for polarization-sensitive measurements is the need to polarize the incident photon beam by scattering from a production target before it can be used for the actual scattering experiment [10]. The associated collimation of the photons, required to form a beam, both at the point of initial emission from the γ source and after the polarizer target, results in a low beam flux. This restricted the “photon-hungry” study of the polarization features of the scattering process to scenarios in which either the angle-differential cross section of a linearly polarized incident beam or the polarization of the scattered radiation resulting from an unpolarized incident beam is measured. However, the introduction of highly polarized, high-intensity photon sources, such as third-generation synchrotrons and free-electron lasers, in combination with novel, highly efficient hard-x-ray polarimeters [11–13], allowed us to overcome these limitations and led to a renewed interest in the polarization-related features of elastic x-ray scattering [14–17]. This motivated a first-of-its-kind experiment at the PETRA III synchrotron, in which the polarization characteristics of both the incident and the outgoing photons were simultaneously investigated at an energy of $\hbar\omega = 175$ keV [18].

*wilko.middents@uni-jena.de

Published by the American Physical Society under the terms of the [Creative Commons Attribution 4.0 International license](https://creativecommons.org/licenses/by/4.0/). Further distribution of this work must maintain attribution to the author(s) and the published article’s title, journal citation, and DOI.

Scattering studies using highly polarized incident radiation also afford the intriguing possibility to exploit the different polarization-dependent characteristics of the various scattering processes. This might provide a new experimental access to Delbrück scattering, which was first mentioned in a commentary on a publication by Meitner and Kösters [2] and is known today as one of the most fundamental nonlinear quantum electrodynamics processes [19]. In the past, various efforts were made to observe Delbrück scattering experimentally by elastically scattering unpolarized high-energy photons on atoms and measuring the cross section [20]. In these studies, good agreement between experimental results and theoretical calculations of the scattering cross section was only achieved when the Delbrück component was taken into account for the total elastic scattering cross section. In a recent theoretical work by Koga and Hayakawa it was proposed to use a highly linearly polarized γ -ray beam and a specific scattering geometry to maximize the relative contribution of Delbrück scattering [21]. This could open up a much improved experimental access for studies of Delbrück scattering, in particular in the energy range where it makes only a small contribution to the total elastic scattering cross section.

The measurement scheme proposed by Koga and Hayakawa motivated us to perform a follow-up study to the pioneering experiment described in [18], the results of which are presented in the following. In addition, we include up to now unpublished data from the previous measurement [18] in the present study. While the previous experiment addressed the polarization characteristics of elastically scattered, highly linearly polarized hard x rays, the present work focuses on the emission pattern of the scattered radiation both within and out of the polarization plane defined by the propagation direction and the polarization of the incident photon beam. Measurements of this kind provide the most detailed probe of our understanding of the elastic scattering process. With an incident photon energy of 175 keV, the present study addresses an energy regime where Rayleigh scattering is still by far the dominant interaction process and we are consequently able to compare the experimental findings to a state-of-the-art treatment of the Rayleigh process. Such a detailed probe of our theoretical understanding of this contribution is crucial for correctly predicting and interpreting the scattering signal in future experiments at higher photon energies where Delbrück scattering becomes non-negligible.

II. THEORETICAL BACKGROUND

In order to investigate the elastic scattering of synchrotron x rays by atomic targets, we start by defining the geometry of this process. As seen from Fig. 1, the (z) quantization axis is taken along the wave vector of the incident photon. For experiments at synchrotron facilities, it is convenient to define the x - z reference (laboratory) plane as the plane of the synchrotron ring that gives rise to emission of the synchrotron light.

For our choice of the reference frame, two angles θ and φ are needed to describe the propagation direction of a scattered photon. The polar angle θ is defined with respect to the z axis. In turn, the azimuthal angle φ characterizes the tilt of the scattering plane with respect to the reference plane, where

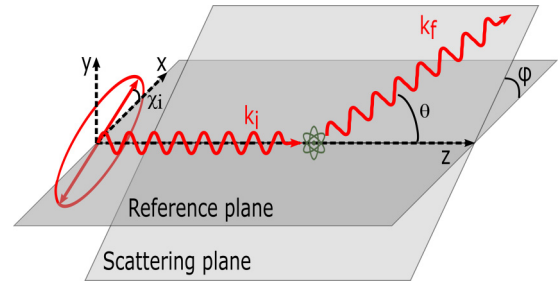


FIG. 1. Geometry of the Rayleigh scattering of a linearly polarized synchrotron beam. Incident photons with wave vector \mathbf{k}_i propagate along the z axis. The plane of the synchrotron ring is denoted by the reference plane x - z . The wave vectors of the incident and scattered photon beams span the scattering plane. The polarization of the incident synchrotron radiation is defined by the ellipse of polarization whose major semi-axis spans the tilt angle χ_i with the reference plane

the scattering plane is spanned by the wave vectors of incident and outgoing photons \mathbf{k}_i and \mathbf{k}_f .

The polarization of the incident photon beam can be conveniently described by two Stokes parameters $P_{1,i}$ and $P_{2,i}$. These parameters are defined by means of intensities of light I_{χ_i} , linearly polarized under a particular angle χ_i with respect to the reference plane, i.e., the plane of the synchrotron ring. Alternatively, $P_{1,i}$ and $P_{2,i}$ can be used to represent the ellipse of polarization. The relative length of the principal axis of this ellipse, $P_{1,i} = \sqrt{P_{1,i}^2 + P_{2,i}^2}$, is the degree of linear polarization of light. The tilt of the principal axis with respect to the reference plane is characterized by the angle $\chi_i = 1/2 \arctan(P_{2,i}/P_{1,i})$ (see Fig. 1 for a representation of $P_{1,i}$ and χ_i). Both definitions of the Stokes parameters can be summarized as

$$P_{1,i} = \frac{I_{0^\circ} - I_{90^\circ}}{I_{0^\circ} + I_{90^\circ}} = P_{1,i} \cos(2\chi_i),$$

$$P_{2,i} = \frac{I_{45^\circ} - I_{135^\circ}}{I_{45^\circ} + I_{135^\circ}} = P_{1,i} \sin(2\chi_i). \quad (1)$$

Although the synchrotron radiation is usually linearly polarized within the reference plane and hence $P_{2,i}$ and χ_i are expected to be 0, we leave both as free parameters which are determined in the experiment.

Having defined the geometry of the elastic photon scattering, we are ready to study the angle-differential cross section of this process:

$$\left(\frac{d\sigma}{d\Omega}\right)_R = |A(\theta, \varphi)|^2. \quad (2)$$

Here $A(\theta, \varphi)$ is the scattering amplitude [5,8,14,22,23]. For the scattering of light by a closed-shell system, i.e., spherically symmetric atom, the scattering amplitude can be parametrized by two linearly independent components A_{\parallel} and A_{\perp} (see Ref. [10]). These components correspond to the cases when incoming and outgoing photons are polarized either parallel or perpendicular to the scattering plane. In terms of A_{\parallel} and A_{\perp} , the angle-differential cross section of elastic scattering for a

linearly polarized incident photon beam is expressed as

$$\left(\frac{d\sigma}{d\Omega}\right)_R = \frac{1}{2}(|A_{\parallel}|^2 + |A_{\perp}|^2) + \frac{1}{2}(|A_{\parallel}|^2 - |A_{\perp}|^2) \times [P_{1,i} \cos(2\varphi) + P_{2,i} \sin(2\varphi)]. \quad (3)$$

By inserting the Stokes parameters (1) into Eq. (3) we can express the angular distribution in terms of the degree of the linear polarization $P_{1,i}$ and the polarization tilt angle χ_i of the incident photon beam

$$\left(\frac{d\sigma}{d\Omega}\right)_R = \frac{1}{2}(|A_{\parallel}|^2 + |A_{\perp}|^2) + \frac{1}{2}(|A_{\parallel}|^2 - |A_{\perp}|^2)P_{1,i} \cos(\chi_i - \varphi). \quad (4)$$

At the photon energies relevant to this work, the elastic scattering cross section is by far dominated by the Rayleigh channel. Since the calculation of the scattering amplitudes has been discussed in detail in the literature (see, for example, [10,14–16]), here we just briefly recall the basic concepts necessary for the scope of this work. State-of-the-art calculations of the scattering amplitudes are performed in a fully relativistic framework, where the electron-photon interaction is treated perturbatively. These scattering amplitudes contain the summation over the complete atomic spectrum, including positive and negative continua, and therefore the calculations are a very complicated task. To overcome this problem, we use the Green's-function approach, which enables us to represent this summation in a closed form as a combination of regular and irregular solutions of the inhomogeneous Dirac equation with a local Dirac-Fock potential [14,24]. In order to describe the photon scattering by a many-electron atom, we employ the independent-particle approximation. In this model, scattering from each single electron in the target atom is calculated independently while the other electrons are considered to be frozen. The total scattering amplitudes are obtained as a sum of the single-electron amplitudes of the electrons from all occupied shells. For high-energy photons and heavy targets this so-called independent-particle approximation works very well [7,10,22]. By considering the sum up to a certain electron shell, the influence of the individual constituents can also be explored [14]. One can show, in particular, that inner-shell electrons provide a dominant contribution to scattering for high scattering angles, which are associated with larger momentum transfers, while for small scattering angles the contributions from higher shells become more important [14].

III. EXPERIMENT

The present measurement was conducted at the High Energy Materials Science beam line P07 of the PETRA III synchrotron facility at DESY, Germany [25]. Before the photon beam entered the experimental hutch, a double-crystal monochromator was used to set its energy to $\hbar\omega = 175$ keV. Subsequently, the beam was collimated to a size of 1×1 mm² and coupled into an evacuated target chamber via a stainless-steel window with a thickness of 50 μ m. A gold foil target with a thickness approximately equal to 1 μ m was positioned in the beam path. The radiation scattered by this target, together with its characteristic lines, was recorded by a

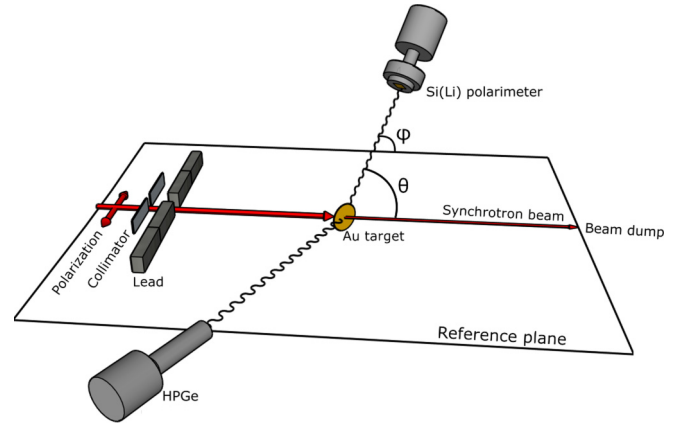


FIG. 2. Schematic view of the experimental setup. The radiation scattered within the gold foil target was recorded by a HPGe detector positioned in the reference (synchrotron) plane of the incident beam, as well as by a Si(Li) detector placed both in and out of the reference plane under different scattering angles. After the collimator the beam is coupled into an evacuated target chamber, which is not visible in this sketch. Lead shielding behind the collimator was installed to prevent radiation scattered by the collimator from entering the detectors.

conventional high-purity germanium (HPGe) x-ray detector as well as a segmented lithium-drifted silicon [Si(Li)] detector. These detectors were positioned at various viewpoints of the target chamber which were equipped with stainless-steel x-ray windows of 50 μ m thickness. To prevent stray radiation produced in the collimator at the entrance of the hutch as well as in the stainless-steel window at the entrance of the experimental setup from reaching the detectors (as observed in [26]), this area was extensively shielded with lead bricks. Moreover, the part of the primary beam not interacting with the target was passing through an evacuated beam tube to the adjacent experimental hutch, where a dedicated beam dump was located. Note that suppression of stray radiation is of critical importance for this type of experiment, as only a very small fraction of all secondary x rays produced within the experimental setup stems from the interaction process of interest, i.e., the elastic scattering within the target foil. A schematic drawing of the experimental setup is presented in Fig. 2.

The Si(Li) detector had an active area of 32×32 mm² and a crystal thickness of approximately 9 mm. This detector system was placed at various positions within and tilted against the reference (synchrotron) plane, defined by the observation angles θ and φ (see Fig. 2). In contrast, the HPGe detector, having a diameter of 49.7 mm and a thickness of 21.1 mm, was positioned solely within the reference plane ($\varphi = 0^\circ$), at various observation angles θ . Both detectors were positioned at a distance of roughly 50 cm from the gold foil target. The preamplifier signals from the detectors were further amplified and subsequently processed by standard analog and digital readout electronics based on the VME and NIM standards. Two exemplary spectra, stemming from each of the two detector systems located at an observation angle of 63° within the reference plane, are presented in Fig. 3. All distinct features in the recorded spectra can be attributed to either scattering

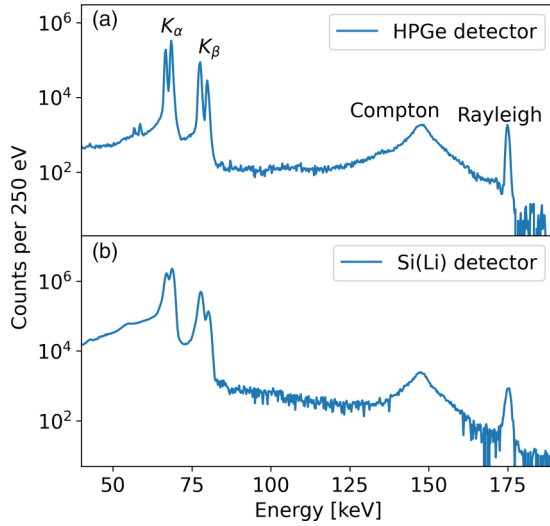


FIG. 3. Energy spectra of 175-keV photons scattered on a gold target measured with different detectors: (a) example spectrum measured with a HPGe detector and (b) spectrum taken with a Si(Li) detector. Both shown spectra are measured at the same position $\theta = 63^\circ$ and $\varphi = 0$. Dominant spectral components are labeled in (a).

processes of the primary x rays within the target foil, i.e., Compton scattering and elastic (Rayleigh) scattering, or the emission of characteristic radiation upon photoabsorption of the primary radiation by a target atom. While the elastic scattering peak appears at the energy of the primary beam of $\hbar\omega = 175$ keV, the Compton peak is shifted to lower energies due to the inelastic nature of this scattering process. The different relative intensities of the respective peaks in the two spectra result from the different energy-dependent detection efficiencies $\eta(\hbar\omega)$ of both detectors.

A list of the various detector positions used in the measurement is presented in Table I. Note that in the present work we also include so far unpublished cross-section data from a measurement [18,26], which was performed in 2014 at the same beamline P07 of the PETRA III facility with the same photon energy ($\hbar\omega = 175$ keV) using a similar experimental

TABLE I. Overview of the detector positions for the present (2020) and previous (2014) beamtimes. The positions are defined by pairs of their polar and azimuthal scattering angles (θ , φ) as defined in Figs. 1 and 2. For the beamtime of 2014 conducted in the framework of [18,26] the positions have an uncertainty of 1° in both θ and φ . For the recent beamtime of 2020 the uncertainty for the polar scattering angle θ is 0.1° and the uncertainty for the azimuthal scattering angle φ is 1° .

Beamtime 2014		Beamtime 2020	
HPGe	Si(Li)	HPGe	Si(Li)
(30°, 0)	(65°, 0)	(38.7°, 0)	(63.4°, 0)
(90°, 0)	(90°, 0)	(63.3°, 0)	(65.2°, 158°)
(135°, 0)	(120°, 0)	(87.6°, 0)	(71.7°, 133°)
(150°, 0)		(113.7°, 0)	(88.2°, 161°)
			(89.1°, 136°)

setup. The corresponding detector positions for this previous beamtime are also included in Table I. The important difference is that in the previous experiment only scattering within the reference plane was observed.

In general, the accuracy of the stated observation angles is about $\pm 1^\circ$, which is due to the limited mechanical precision of the positions of the x-ray window flanges mounted on the target chamber. However, the value of the polar scattering angle θ can be independently determined from the position of the Compton peak in the corresponding x-ray spectra. Indeed, by using the relation $\hbar\omega' = \hbar\omega/[1 + \frac{\hbar\omega}{m_e c^2}(1 - \cos\theta)]$, where $\hbar\omega$ and $\hbar\omega'$ are the energies of the incident and Compton scattered photons, respectively, the polar scattering angle can be determined with a reduced uncertainty of $\Delta\theta = 0.1^\circ$.

IV. DATA ANALYSIS AND DISCUSSION

To obtain angle-differential cross sections for Rayleigh scattering $(d\sigma/d\Omega)_R$ we employed a normalization method for each individual spectrum. To be more specific, the Rayleigh cross section can be expressed in terms of the production cross section of the characteristic K_α radiation σ_K by normalizing the intensity I_R of the Rayleigh peak to the intensity I_K of the isotropic K_α radiation

$$\left(\frac{d\sigma}{d\Omega}\right)_R = \frac{I_R}{I_K} \frac{\eta_K}{\eta_R} \frac{\sigma_K}{4\pi}, \quad (5)$$

with η_K and η_R being the photopeak efficiencies of the x-ray detectors at the energies of the K_α and Rayleigh peak, respectively. Similar relative cross-section determinations were also performed in Refs. [27–29]. The estimation of the Rayleigh cross section is now linked to the cross section of K_α emission σ_K that can be calculated as

$$\sigma_K = \sigma_{\text{ion},K} \omega_K p(K_\alpha), \quad (6)$$

with the photoionization cross section of the K -shell electrons $\sigma_{\text{ion},K}$, the atomic radiative yield of the K shell ω_K [30], and the ratio p of the relative intensities of the K_α and the K_β lines [31]. Via this normalization procedure, several sizable systematic uncertainties such as the solid angle covered by each of the x-ray detectors, possible fluctuations in the incident photon beam flux, and the exact target thickness are canceled.

The intensities I_K and I_R are obtained from the recorded spectra by performing a χ^2 fit to the K_α and Rayleigh peaks using a combination of a Gaussian line profile and detector-dependent correction terms as presented in [32]. Additionally, a linear background term is included. As the real shape of the peaks is not known, the fitting procedure is performed for different combinations of the correction terms which result in a reasonable representation of the peaks. An example of the fitting procedure for the Rayleigh peak is shown in Fig. 4. The line intensity is calculated as the mean of the different results of the fitting procedures. The uncertainty of the obtained line intensities results from a combination of the statistical uncertainty and the uncertainty of the fitting routine itself. The latter part of the uncertainty is estimated by the maximal difference between the results of the different fitting procedures and their mean value.

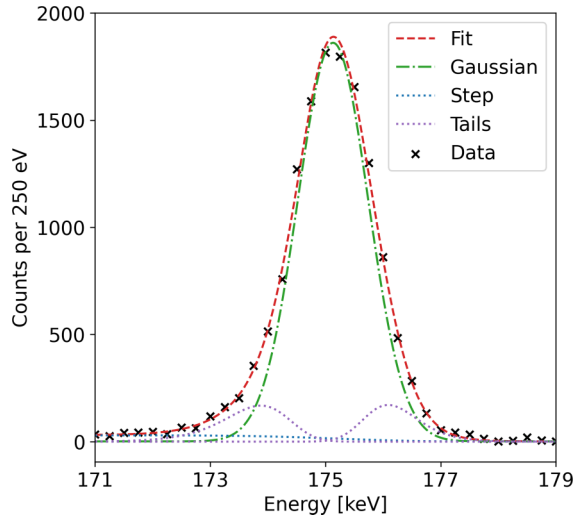


FIG. 4. Example of fitting the model function to the energy region of the Rayleigh peak. The fitting function consists of a Gaussian and several correction terms. In this example the peak shape is corrected by a step function and a tail function on both the low- and high-energy sides of the peak.

The cross section for the ionization of a *K*-shell electron in gold by 175-keV x rays was calculated to be $\sigma_{\text{ion},K} = 293$ b with an uncertainty of 5%. The calculations were performed within a fully relativistic approach. In this approach the wave functions of both bound and continuum electron states are solutions of the Dirac equation with the screening Dirac-Fock potential, and higher-order multipoles of the radiation field are taken into account.

The EGS5 Monte Carlo code for photon and electron transport in matter [33] was used to obtain the detector efficiency factors η for both the Ge detector and the Si(Li) polarimeter. As shown previously [34], all relevant features of the detector response can be reproduced by this code. The uncertainty of the efficiency correction is estimated conservatively to be 5%. Due to the uncertainties in the photoionization cross section and the efficiency correction, the overall systematic uncertainty of the determination of the angle-differential scattering cross sections is estimated by the quadratic sum of the individual constituents to be 8%.

In the following we first present the Rayleigh cross-section values obtained for scattering within the plane of the synchrotron ring. These values were obtained both in previous work [18,26] and in our recent experiment. Afterward, we show the data of the present experiment where detectors were also positioned outside the synchrotron plane.

A. Rayleigh scattering within the synchrotron plane

In both experiments, Rayleigh scattering within the plane of the synchrotron ring was analyzed. The incident synchrotron radiation, set to a photon energy of 175 keV, is known to be strongly linearly polarized within the synchrotron plane. We assume the polarization of the incident synchrotron beam not to differ significantly between the two beamtimes, as both experiments were performed at the same beamline with a similar setup and all variables, such as the photon energy, were the same. In both experiments, the synchrotron radiation was

scattered by a thin gold foil target. In Fig. 5(a) we present the results of both experiments, showing the angle-differential cross sections of Rayleigh scattering of a 175-keV highly linearly polarized synchrotron beam by a gold foil target for different scattering angles θ . As can be seen from this figure, the angle-differential cross section is large for small and large scattering angles and exhibits a dip for $\theta \approx 90^\circ$. This behavior is well confirmed by the experimental results obtained in both measurements.

In order to elucidate the experimental results for the angle-differential cross section, displayed in Fig. 5(a), we employ the theory from Sec. II. Note, however, that Eqs. (3) and (4) were obtained under the assumption that photons are scattered by spherically symmetric atoms with total angular momentum $J = 0$, while our experiments were performed for the gold atom, whose ground-state electronic configuration is $[\text{Xe}]4f^{14}5d^{10}6s$. In order to justify the use of the obtained equations, we investigated theoretically the contributions of individual atomic shells to the angle-differential cross section. In Fig. 5(b) we present the angle-differential cross sections for different shells of the gold atom. Theoretical curves are shown for scattering from the *K* (dotted line), *KL* (dash-double-dotted line), *KLM* (dash-dotted line), and *KLMN* (dashed line) shells as well as for the contribution from all occupied shells (solid line). As seen from the figure, the role of various atomic shells varies significantly with the scattering angle θ . For $\theta > 120^\circ$, for example, the dominant contribution to the angle-differential cross section is due to the *K*-shell scattering. This is expected from the fact that large momentum transfer is involved in the backward scattering. At smaller angles, and hence for smaller momentum transfer, the scattering from higher electron shells becomes more important. For the forward scattering angles $\theta < 30^\circ$, for example, the differential cross section is enhanced by more than an order of magnitude if higher shells up to the *O* shell are taken into account. However, for the angular range $30^\circ < \theta < 150^\circ$, covered in both our experiments, the dominant contributions to the Rayleigh scattering are provided by the *K*, *L*, and *M* shells, while the effect of the higher shells does not exceed 1%. These predictions justify the use of the expressions (3) and (4), derived for the closed-shell systems, for the analysis of the x-ray scattering by gold atoms as in our experiment only scattering for $\theta \geq 30^\circ$ was analyzed.

For the case when the scattered photons are detected within the reference (synchrotron) plane where $\varphi = 0$, Eq. (3) can be simplified to

$$\left(\frac{d\sigma}{d\Omega}\right)_R = \frac{1}{2}(|A_{\parallel}|^2 + |A_{\perp}|^2) + \frac{1}{2}(|A_{\parallel}|^2 - |A_{\perp}|^2)P_{1,i}. \quad (7)$$

Based on this expression, we can understand, at least qualitatively, the experimentally observed angular distribution. Indeed, by assuming the incident light to be almost completely linearly polarized $P_{1,i} \approx 1$, one can estimate the differential cross section as

$$\left(\frac{d\sigma}{d\Omega}\right)_R \approx |A_{\parallel}|^2. \quad (8)$$

Using the form-factor approximation $A_{\parallel} = A_{\perp} \cos \theta$ [22], we can see that no emission should be observed around $\theta \approx 90^\circ$. The same can also be expected from any other semiclassical

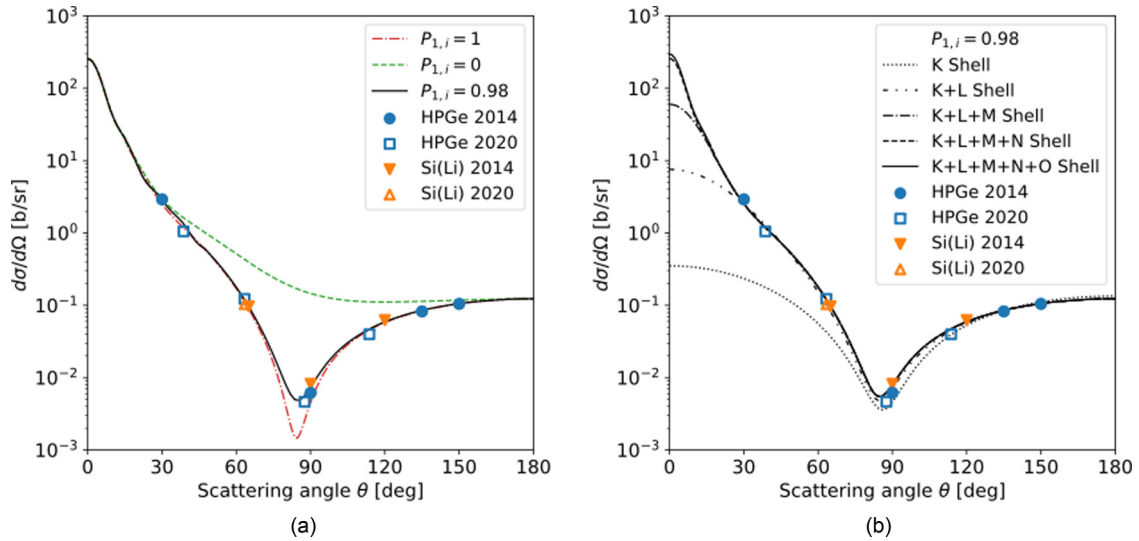


FIG. 5. Angular distribution of Rayleigh scattering of 175-keV x rays on gold within the synchrotron plane. Data from both measurements are shown. The data acquired with the HPGe detector are marked with closed blue circles (data from 2014) and open blue squares (data from 2020) and the data acquired with the Si(Li) detector are marked with closed orange downward-pointing triangles (2014) and open orange upward-pointing triangles (2020). Due to the size of the markers and of the y scale, the uncertainty of the experimental data is not visible. The theoretical lines are calculated in the independent-particle approximation. (a) Calculations for a completely linearly polarized ($P_{1,\text{in}} = 1$) and an unpolarized ($P_{1,\text{in}} = 0$) incident synchrotron beam as well as for an incident beam with the Stokes parameters $P_{1,i} = 0.98$ and $P_{2,i} = 0$. (b) For the presented theoretical curves, the scattering amplitudes are calculated within the IPA theory when including scattering from the K, KL, KLM, KLMN, and KLMNO shells for a Stokes parameter $P_{1,i} = 0.98$.

approach [5]. However, the experimental results show that even for the “forbidden” angle $\theta = 90^\circ$, a finite value is obtained for the angle-differential cross section. Additionally, the minimum of the angular distribution is shifted towards a lower polar angle. The deviations of the experimental results are due to the relativistic and many-body effects that are not accounted for in the form-factor approximation.

To account for these nonclassical effects, we additionally compared the experimental findings with (more accurate) theoretical predictions, based on the relativistic independent-particle approximation (IPA). This approximation was employed in order to calculate the scattering amplitudes A_{\parallel} and A_{\perp} for the K, L, M, N, and O shells which were subsequently used to calculate the angle-differential cross section according to Eq. (7). In addition to the relativistic effects, which are accounted for by the IPA, the angle-differential cross section is also influenced by the degree of linear polarization of the incident radiation. In Fig. 5(a) we additionally present theoretical predictions for the angle-differential cross section. The theoretical angular distribution for an incident fully linearly polarized beam, $P_{1,i} = 1$, also shows a strong decrease for the photon emission perpendicular to the z axis while remaining at a finite value at the classically forbidden angle $\theta = 90^\circ$. However, this theoretical curve does not completely reproduce the experimental data. Especially for the region around a polar scattering angle $\theta = 90^\circ$, the measured angle-differential cross sections are almost an order of magnitude larger than expected. This deviation can be explained by a small depolarization of the incident beam, leading to a stronger influence of the scattering amplitude A_{\perp} which corresponds to scattering of the part of the incident beam being polarized perpendicular to the scattering plane. In our previous study [18], the Stokes parameter $P_{1,i}$ of the incident

synchrotron beam was determined by using the polarization of the radiation being Compton scattered off the gold foil target to be $P_{1,i} = 0.980 \pm 0.009$ (and additionally by means of the polarization of the radiation being Rayleigh scattered of the gold foil target to be $P_{1,i} = 0.982 \pm 0.009$). Using this value ($P_{1,i} = 0.98$) for the polarization of the incident beam, we plotted an additional theoretical prediction for the angle-differential cross section in Fig. 5(a). It can be seen that good agreement between the experimental data and theoretical values is achieved when considering this small (just 2%) depolarization of the incident beam.

B. Azimuthal-angle dependence of Rayleigh scattering

In the present experiment at PETRA III we extended the previous study by also analyzing the angle-differential cross section for Rayleigh-scattered radiation out of the reference plane, i.e., for $\varphi \neq 0$. The results of the cross-section analysis according to Eq. (5) are displayed in Fig. 6 for the three cases of $\varphi \approx 0, 160^\circ, 135^\circ$. For neighboring azimuthal scattering angles, the data were plotted in the same plot for better visualization. As can be seen from the figure, the dependence of the angle-differential cross section on the polar angle θ is strongly sensitive to the azimuthal angle φ . The previously described strong dip around $\theta = 90^\circ$ is strongly reduced for $\varphi \approx 160^\circ$ and almost disappears at $\varphi \approx 135^\circ$.

Similar to Sec. IV A, we again employed Eqs. (3) and (4) in order to obtain theoretical predictions that can be compared to the experimental findings. Again, the scattering amplitudes A_{\parallel} and A_{\perp} were calculated within the IPA for scattering by the K, L, M, and N shells. As already mentioned above, scattering from higher shells was neglected, as this only becomes a contributing factor for small scattering angles $\theta < 30^\circ$. As

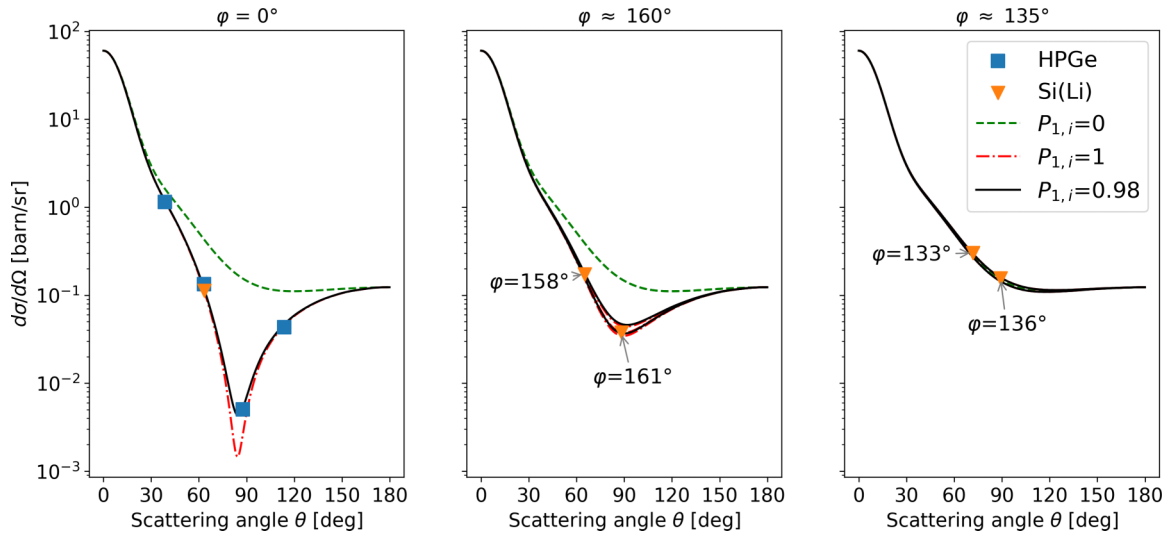


FIG. 6. Angle-differential cross sections for Rayleigh scattering a 175-keV highly linearly polarized synchrotron beam on gold for different azimuthal scattering angles. The experimental data are obtained with a high-purity germanium detector (blue squares) and a two-dimensional sensitive Si(Li) Compton polarimeter (orange triangles). Additionally, the theoretical prediction for the angular distribution is plotted for a fully linearly polarized incident synchrotron beam (red dash-dotted lines), a completely unpolarized synchrotron beam (green dashed line), and an incident synchrotron beam with the Stokes parameters $P_{1,i} = 0.982$ and $P_{2,i} = 0$ (black solid lines). In the plots for $\varphi > 0$, theory curves are plotted for each azimuthal scattering angle corresponding to a data point.

seen from Eq. (3) and our discussion above, the angle-differential cross section of Rayleigh scattering depends not only on the polar angle θ and azimuthal angle φ but also on the linear polarization of the incident radiation in terms of the Stokes parameters $P_{1,i}$ and $P_{2,i}$. In Fig. 6 we display also our calculations for different parameters $P_{1,i}$, while we limit ourselves to the case $P_{2,i} = 0$. We present the calculation for a completely unpolarized beam, meaning $P_{1,i} = 0$ (green dashed line), an incident beam which is completely linearly polarized in the synchrotron plane $P_{1,i} = 1$ (red dash-dotted line) and for an incident beam with $P_{1,i} = 0.98$ (black solid line). For the coplanar geometry case $\varphi = 0$, theoretical predictions, based on these three sets of polarization parameters, significantly differ from each other for the angle around $\theta = 90^\circ$. We recall that we already observed this in Sec. IV A and that calculations for $P_{1,i} = 0.98$ are in the best agreement with experimental data, indicating a small polarization impurity of the synchrotron radiation. However, with an increasing azimuthal angle φ , the difference between the theoretical results becomes less remarkable and for $\varphi = 135^\circ$ (and also for $\varphi = 45^\circ$) all three curves become indistinguishable. This behavior can be easily understood based on Eq. (3), which for $\varphi = 135^\circ$ and $P_{2,i} = 0$ suggests that the angle-differential cross section is independent of the polarization of incident synchrotron radiation.

The experimental results obtained from the present measurement are summarized in Table II. Apart from the experimentally obtained values, we additionally present the theoretical predictions, obtained for the Stokes parameters of the incident synchrotron radiation $P_{1,i} = 0.982 \pm 0.009$ and $P_{2,i} = 0$. In contrast to the theoretical results presented in Fig. 6, where a pointlike detector was assumed, here the finite size of the detector crystals was considered. Due to the size of the detector crystal, the detector covers a certain finite opening angle dependent on the distance of the detector

to the target. To account for the finite size of the detector crystals, the scattering amplitudes were integrated over the opening angle corresponding to the detector surface. The uncertainties for the theoretically predicted cross sections take into account uncertainties in the polar and azimuthal scattering angles under which the detector is positioned and the uncertainty in the polarization of the incident beam according to its Stokes parameters $P_{1,i}$. The experimental data and the theoretical predictions show good agreement when the error bars are considered. The strong polarization sensitivity of the angle-differential cross sections around $\theta = 90^\circ$ amplifies the uncertainty of the Stokes parameters of the incident radiation leading to the large error bars for the theoretical data, especially for $\varphi = 0$.

The high polarization sensitivity of the angle-differential cross section can conversely be used to determine the polarization of the incident beam. By fitting Eq. (4) to the experimental data of the present beam time, we determined the Stokes parameters of the incident synchrotron beam as free fitting parameters. In order to account for the systematic uncertainty of the experimental data given by the uncertainties in the detector efficiency and the ionization cross section, an additional fitting parameter was introduced, which was multiplied by the experimental data. The resulting angular distribution and the experimental data are shown in Fig. 7. In the figure, the theoretical angular distribution is shown for a pointlike detector, while the fitting procedure took into account the finite detector size. For better visualization, theoretical curves for similar azimuthal scattering angles are depicted in the same style. The resulting Stokes parameters of the incident beam are $P_{1,i} = 0.988 \pm 0.004$ and $P_{2,i} = 0.023 \pm 0.047$. This result agrees well with the reference value for the synchrotron polarization obtained in Ref. [18]. Thus, by analyzing the angular scattering distribution of Rayleigh scattering, the polarization of the incident

TABLE II. Angle-differential Rayleigh scattering cross sections $(d\sigma/d\Omega)_R(\theta, \varphi)$. Apart from the shown statistical errors in the determination of the values, the experimental data are influenced by a systematic error of in total 8%, as discussed in the text. Theoretical calculations assume Stokes parameters of the incident beam of $P_{1,i} = 0.982 \pm 0.009$ and $P_{2,i} = 0$, as provided by [18]. The errors of the theoretical predictions include an uncertainty in $P_{1,i}$, which influences all values in a similar direction and the uncertainties in both θ and φ .

Detector	Scattering angles		Experiment (mb sr ⁻¹)	Theory (mb sr ⁻¹)
	θ (deg)	φ (deg)		
Ge	38.7	0	1052 (73)	1192 (47)
Ge	63.3	0	122.7 (69)	122.0 (83)
Ge	87.6	0	4.64 (38)	6.0 (14)
Ge	113.7	0	39.7 (36)	46.6 (11)
Si(Li)	63.4	0	103.7 (47)	121.0 (83)
Si(Li)	65.2	158	159.3 (82)	173 (11)
Si(Li)	71.7	133	277.8 (84)	294 (11)
Si(Li)	88.2	161	34.7 (31)	36.9 (34)
Si(Li)	89.1	136	143.9 (72)	144.1 (53)

synchrotron beam can be determined with high accuracy. A clear advantage of this approach is the simplicity of the setup, as only a thin target foil and a standard x-ray detector are necessary. Additionally, due to the higher statistics in cross-section measurements compared to the polarization analysis presented in Ref. [18], similar if not improved accuracy can be realized in significantly shorter acquisition times.

V. CONCLUSION AND OUTLOOK

We studied the angular distribution for Rayleigh scattering of a linearly polarized synchrotron beam on a thin gold foil target. When including a slight depolarization of the incident beam, as was already determined in a previous study [18], in the theoretical prediction, good agreement between the experimentally measured cross sections and the theoretical predictions is found when calculations of the scattering amplitudes A_{\parallel} and A_{\perp} are performed within the IPA model. In this work an intense hard-x-ray beam generated at a third-

generation synchrotron facility PETRA III at DESY was used to analyze Rayleigh scattering both within and out of the reference plane. The incident beam is highly linearly polarized within the reference plane with well-known polarization characteristics. In this study of hard-x-ray Rayleigh scattering, the polarization of the incident beam is well known and scattering both within and out of the reference plane is measured. Analyzing the angular distribution of Rayleigh scattering alone already serves as a stringent test of the underlying theory. We leave for future work the analysis of the polarization of the Rayleigh scattered radiation.

Furthermore, relying on the experimental findings and theoretical angle-differential cross sections, the analysis of the angular distribution can serve as a highly precise tool for the polarization diagnostics of highly polarized photon beams at high photon energies of up to several hundred keV. A strong advantage is the rather simple setup as only a thin target foil has to be placed in the primary beam. This would even allow for an online diagnostic during the ongoing experiment if the polarization diagnostic is performed in a previous part of the beamline or for a permanent installation at the beamline. In [18] it was suggested to analyze the polarization of the Rayleigh-scattered radiation for the polarization diagnostic of the incident beam. While this method can be also very precise, a drawback of it would be the much higher statistics needed for the polarization measurement compared to the angle-differential cross-section determination making the polarization-based method much slower. Additionally, analyzing the angular distribution of Rayleigh scattering does not rely on the use of complex custom-made detector setups like the Compton polarimeters. The use of a standard HPGc detector positioned under a polar scattering angle around $\theta \approx 90^\circ$ would be sufficient, while a much more accurate diagnostic would be possible when analyzing the angular distribution under multiple scattering angles. When also changing the azimuthal scattering angle, not only the Stokes parameter $P_{1,i}$ but also Stokes parameter $P_{2,i}$ of the incident beam can be controlled. As precise knowledge of the polarization of the incident photon source is very important for precision experiments at high-power photon facilities, a highly precise polarization diagnostic of the incident beam provides valuable insight.

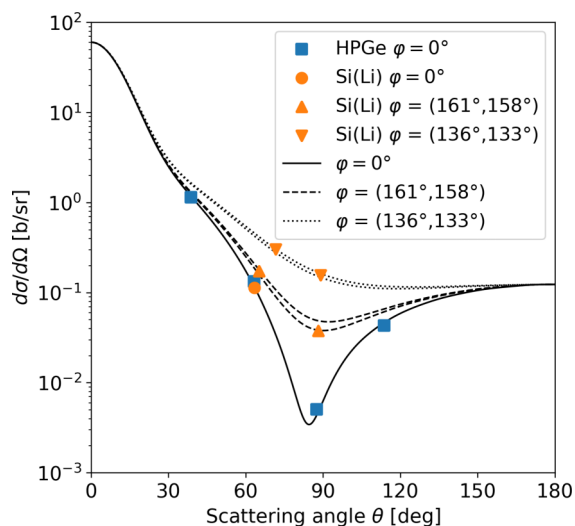


FIG. 7. Fit of the angular scattering distribution of Rayleigh scattering to the experimental data. The Stokes parameters $P_{1,i}$ and $P_{2,i}$ are used as fitting parameters.

ACKNOWLEDGMENTS

The authors acknowledge financial support from the German Federal Ministry of Education and Research (BMBF) under Grant No. 05P15SJFAA. W.M. acknowledges funding from BMBF via Verbundforschung Grant No. 05P19SJFAA. M.V. acknowledges funding from BMBF via Verbund-

forschung Grant No. 05P18SJRB1. Support from the SPARC collaboration is acknowledged. Parts of this research were carried out at the light source PETRA III at DESY, a member of the Helmholtz Association (HGF). Support from the GSI target laboratory and the GSI Department of Experiment Electronics is acknowledged.

-
- [1] W. Franz, Rayleighsches streuung harter strahlung an schweren atomen, *Z. Phys.* **98**, 314 (1935).
- [2] L. Meitner and H. Kösters, Über die streuung kurzwelliger γ -strahlen, *Z. Phys.* **84**, 137 (1933).
- [3] Z. Berant, R. Moreh, and S. Kahane, Nuclear Thomson scattering of 5.5–7.2 MeV photons, *Phys. Lett. B* **69**, 281 (1977).
- [4] E. Fuller and E. Hayward, The nuclear photoeffect in holmium and erbium, *Nucl. Phys.* **30**, 613 (1962).
- [5] P. P. Kane, L. Kissel, R. H. Pratt, and S. C. Roy, Elastic scattering of γ -rays and X-rays by atoms, *Phys. Rep.* **140**, 75 (1986).
- [6] D. A. Bradley, O. D. Gonçalves, and P. P. Kane, Measurements of photon-atom elastic scattering cross-sections in the photon energy range 1 keV to 4 MeV, *Radiat. Phys. Chem.* **56**, 125 (1999).
- [7] S. Roy, L. Kissel, and R. Pratt, Elastic scattering of photons, *Radiat. Phys. Chem.* **56**, 3 (1999).
- [8] W. R. Johnson and K.-t. Cheng, Elastic scattering of 0.1–1-MeV photons, *Phys. Rev. A* **13**, 692 (1976).
- [9] D. Brini, E. Fuschini, D. S. R. Murty, and P. Veronesi, Rayleigh scattering of polarized photons, *Nuovo Cimento* **11**, 533 (1959).
- [10] S. C. Roy, B. Sarkar, L. D. Kissel, and R. H. Pratt, Polarization effects in elastic photon-atom scattering, *Phys. Rev. A* **34**, 1178 (1986).
- [11] S. Tashenov, T. Stöhlker, D. Banaś, K. Beckert, P. Beller, H. F. Beyer, F. Bosch, S. Fritzsche, A. Gumberidze, S. Hagmann, C. Kozhuharov, T. Krings, D. Liesen, F. Nolden, D. Protic, D. Sierpowski, U. Spillmann, M. Steck, and A. Surzhykov, First Measurement of the Linear Polarization of Radiative Electron Capture Transitions, *Phys. Rev. Lett.* **97**, 223202 (2006).
- [12] G. Weber, K.-H. Blumenhagen, H. Bräuning, H. Ding, S. Fritzsche, S. Hess, R. Martin, U. Spillmann, A. Surzhykov, S. Trotsenko, D. F. A. Winters, V. A. Yerokhin, and T. Stöhlker, Compton polarimetry using double-sided segmented x-ray detectors, *J. Phys.: Conf. Ser.* **583**, 012041 (2015).
- [13] M. Vockert, G. Weber, U. Spillmann, T. Krings, M. O. Herdrich, and T. Stöhlker, Commissioning of a Si(Li) Compton polarimeter with improved energy resolution, *Nucl. Instrum. Methods Phys. Res. Sect. B* **408**, 313 (2017).
- [14] A. Surzhykov, V. A. Yerokhin, T. Stöhlker, and S. Fritzsche, Corrigendum: Rayleigh x-ray scattering from many-electron atoms and ions, *J. Phys. B* **48**, 189501 (2015).
- [15] A. Surzhykov, V. A. Yerokhin, S. Fritzsche, and A. V. Volotka, Diagnostics of polarization purity of x rays by means of Rayleigh scattering, *Phys. Rev. A* **98**, 053403 (2018).
- [16] A. V. Volotka, A. Surzhykov, and S. Fritzsche, Rayleigh scattering of linearly polarized light: Scenario of the complete experiment, *Phys. Rev. A* **102**, 042814 (2020).
- [17] S. Srnat, V. A. Yerokhin, A. V. Volotka, G. Weber, S. Fritzsche, R. A. Müller, and A. Surzhykov, Polarization studies on Rayleigh scattering of hard x rays by closed-shell atoms, *Phys. Rev. A* **103**, 012801 (2021).
- [18] K.-H. Blumenhagen, S. Fritzsche, T. Gassner, A. Gumberidze, R. Martin, N. Schell, D. Seipt, U. Spillmann, A. Surzhykov, S. Trotsenko, G. Weber, V. A. Yerokhin, and T. Stöhlker, Erratum: Polarization transfer in Rayleigh scattering of hard x-rays, *New J. Phys.* **18**, 119601 (2016).
- [19] V. Costantini, B. De Tollis, and G. Pistoni, Nonlinear effects in quantum electrodynamics, *Nuovo Cimento A* **2**, 733 (1971).
- [20] M. Schumacher, Delbrück scattering, *Radiat. Phys. Chem.* **56**, 101 (1999).
- [21] J. K. Koga and T. Hayakawa, Possible Precise Measurement of Delbrück Scattering using Polarized Photon Beams, *Phys. Rev. Lett.* **118**, 204801 (2017).
- [22] L. Kissel, R. H. Pratt, and S. C. Roy, Rayleigh scattering by neutral atoms, 100 eV to 10 MeV, *Phys. Rev. A* **22**, 1970 (1980).
- [23] A. Surzhykov, V. A. Yerokhin, T. Jahrsetz, P. Amaro, T. Stöhlker, and S. Fritzsche, Polarization correlations in the elastic Rayleigh scattering of photons by hydrogenlike ions, *Phys. Rev. A* **88**, 062515 (2013).
- [24] V. A. Yerokhin, Nuclear-size correction to the Lamb shift of one-electron atoms, *Phys. Rev. A* **83**, 012507 (2011).
- [25] N. Schell, A. King, F. Beckmann, T. Fischer, M. Müller, and A. Schreyer, The High Energy Materials Science Beamline (HEMS) at PETRA III, *Mater. Sci. Forum* **772**, 57 (2013).
- [26] K.-H. Blumenhagen, U. Spillmann, T. Gaßner, A. Gumberidze, R. Martin, N. Schell, S. Trotsenko, G. Weber, and T. Stöhlker, Identification and reduction of unwanted stray radiation using an energy- and position-sensitive Compton polarimeter, *Phys. Scr.* **T166**, 014032 (2015).
- [27] T. Stöhlker, T. Ludziejewski, H. Reich, F. Bosch, R. W. Dunford, J. Eichler, B. Franzke, C. Kozhuharov, G. Menzel, P. H. Mokler, F. Nolden, P. Rymuza, Z. Stachura, M. Steck, P. Swiat, A. Warczak, and T. Winkler, Charge-exchange cross sections and beam lifetimes for stored and decelerated bare uranium ions, *Phys. Rev. A* **58**, 2043 (1998).
- [28] J. S. Shahi, S. Puri, D. Mehta, M. L. Garg, N. Singh, and P. N. Trehan, Large-angle elastic scattering of 59.54-keV photons by elements with $12 \leq Z \leq 92$, *Phys. Rev. A* **57**, 4327 (1998).
- [29] S. Puri, B. Chand, D. Mehta, M. Garg, N. Singh, and P. Trehan, Differential cross section measurements for the elastic scattering of 59.5 keV photons by elements in the atomic region $13 \leq Z \leq 82$, *Nucl. Instrum. Methods Phys. Res. Sect. B* **111**, 209 (1996).
- [30] M. O. Krause, Atomic radiative and radiationless yields for K and L shells, *J. Phys. Chem. Ref. Data* **8**, 307 (1979).

- [31] A. Thompson, D. Attwood, E. Gullikson, M. Howells, K.-J. Kim, J. Kirz, J. Kortright, I. Lindau, Y. Liu, P. Pianetta, A. Robinson, J. Scofield, J. Underwood, G. Williams, and H. Winick, *X-Ray Data Booklet*, 3rd ed. (Lawrence Berkeley National Laboratory, Berkeley, 2009).
- [32] R. G. Helmer and M. A. Lee, Analytical functions for fitting peaks from Ge semiconductor detectors, *Nucl. Instrum. Methods* **178**, 499 (1980).
- [33] H. Hirayama, Y. Namito, A. F. Bielajew, S. J. Wilderman, and W. R. Nelson, SLAC Report No. SLAC-R-730, 2005 (unpublished).
- [34] G. Weber, H. Bräuning, R. Märtin, U. Spillmann, and T. Stöhlker, Monte Carlo simulations for the characterization of position-sensitive x-ray detectors dedicated to Compton polarimetry, *Phys. Scr.* **T144**, 014034 (2011).

Correction: Four entries in the last column of Table I have been fixed. Values given for φ in the first and second paragraphs of Sec. IV B and in the third column of Table II have been fixed. Values for P_1 and P_2 in the last paragraph of Sec. IV B have been corrected. The previously published Figures 6 and 7 contained corresponding errors and have been replaced.